

# Numerical simulations of the 1840s great eruption of $\eta$ Carinae

## I. Revisiting the explosion scenario

R. F. González<sup>1</sup>, Luis A. Zapata<sup>1</sup>, A. C. Raga<sup>2</sup>, J. Cantó<sup>3</sup>, P. F. Velázquez<sup>2</sup>, and E. M. de Gouveia Dal Pino<sup>4</sup>

<sup>1</sup> Instituto de Radioastronomía y Astrofísica (UNAM), A.P. 3-72 C.P. 58190 Morelia, Michoacán, México  
e-mail: rf.gonzalez@irya.unam.mx;l.zapata@irya.unam.mx

<sup>2</sup> Instituto de Ciencias Nucleares (UNAM), A.P. 70-543, C.P. 04510, México, México  
e-mail: pablo@nucleares.unam.mx; raga@nucleares.unam.mx

<sup>3</sup> Instituto de Astronomía (UNAM), A.P. 70-264, C.P. 04510, México, México e-mail: jcanto@astro.unam.mx

<sup>4</sup> Instituto de Astronomia, Geofísica e Ciências Atmosféricas (IAG-USP), Rua do Matão, São Paulo 05508-090, Brazil)

Received ; accepted

### ABSTRACT

In this work, we present new two-dimensional hydrodynamical simulations of the major eruption of  $\eta$  Car in the 1840s, which resulted in the formation of a bipolar nebula that is commonly known as the *large* Homunculus. In our numerical models, we have included the high-speed component of  $10000 \text{ km s}^{-1}$ , detected in recent observations, that provides direct evidence of an explosive event. Here, we investigate whether such a violent explosion is able to explain both the shape and the dynamical evolution of  $\eta$  Car's nebula. As in our previous work, we have assumed a two-stage scenario for  $\eta$  Car's eruption: a slow outflow phase during a few decades before the eruption followed by the explosive event. From the collision of these outflow phases, the *large* Homunculus is produced. Our numerical simulations show that such scenario does not resemble some of the observed physical features and the expansion of the nebula. Notwithstanding, we also explore other injection parameters (mass-loss rate and ejection velocity) for these outflow phases. In particular, we find that an explosion with an intermediate-speed of  $1000 \text{ km s}^{-1}$  is able to reproduce the morphology and the kinematical age of the *large* Homunculus.

**Key words.** stars: individual ( $\eta$  Carinae) – stars: winds, outflows – hydrodynamics – shock waves

### 1. Introduction

The origin of the 19th century major eruption of the massive star  $\eta$  Car is still in an intense debate (e.g. Portegies Zwart, & van den Heuvel 2016; Smith 2006). The  $\eta$  Car system is a bright ( $4 \times 10^6 L_{\odot}$ ) and massive stellar system that contains an evolved (Luminous Blue Variable LBV) star with a mass of  $\sim 90 M_{\odot}$  and a less massive ( $\sim 30 M_{\odot}$ ) main sequence star companion. The orbital period of such an eccentric system ( $e = 0.9$ ) is only 5.5 yr (Portegies Zwart, & van den Heuvel 2016). The primary star of  $\eta$  Car's system has undergone several eruptive events, being the most notorious the major eruption in the 1840s (Davidson & Humphreys 1997) during which  $\eta$  Car drastically increased its visual magnitude (Humphreys et al. 1999), and expelled a large amount of mass ( $\geq 10 M_{\odot}$ ) into its surroundings (Smith et al. 2003). From this eruption, a bipolar nebula known as the *large* Homunculus was formed which extends  $\pm 9$  arcsec along the symmetry axis (that corresponds to a physical size of  $\pm 3.25 \times 10^{17} \text{ cm}$  at a distance of 2.3 Kpc) and expands at a speed of  $\sim 650 \text{ km s}^{-1}$  in the polar direction (see, Smith 2006). Its symmetry axis is inclined  $\sim 45^{\circ}$  to the line of sight (Davidson et al. 2001). In addition, there were at least two other outbursts after this event in the years of 1890s and 1940s. From these eruptions the so-called *little* and *baby* Homunculi were produced, respectively (Ishibashi et al. 2003; Abraham et al. 2014).

The most successful explanation of the nature and the origin of the Homunculus nebula is given by the stellar merger model (Portegies Zwart, & van den Heuvel 2016; Smith et al. 2018a). The merger between two massive stars in a triple hierarchical

system could account for most of the physical characteristics observed in  $\eta$  Car. These physical features include the kinetic energy ( $10^{49.6} - 10^{50} \text{ erg}$ ), the luminosity burst ( $4 \times 10^6 L_{\odot}$ ), the bipolar shape of the Homunculus, and the two successive stages of the velocity field during the main eruption: one very broad  $\sim 10000 \text{ km s}^{-1}$ , and the other one of  $\sim 600 \text{ km s}^{-1}$  (Smith et al. 2018a). Nonetheless, there are some other models for explaining the nature of the *large* Homunculus, such as super-Eddington eruptions (Owocki & Shaviv 2016), binary interactions at periastron (Kashi & Soker 2009), and pulsational pair instabilities in a massive star (Woosley 2017), but they do not account for all the observed features in the nebula.

The violent eruption of the mid-nineteenth century suffered by  $\eta$  Car was analogous to a type II supernova explosion, but with lower energy released to the interstellar medium (ISM) ( $E_k \sim 10^{50} \text{ erg}$  over a few years) and therefore, it is referred to as a supernova impostor (Smith 2013). The extremely broad emission wings of about  $\sim 10000 \text{ km s}^{-1}$  in the  $H_{\alpha}$  optical lines are likely caused by high-velocity outflowing material occurred during the explosion (Smith et al. 2018b). In a recent paper, González (2018) investigated through two-dimensional hydrodynamical simulations whether an explosive event is able to explain the shape and kinematics of the *large* Homunculus nebula. These numerical models revealed that in fact the explosion can indeed explain some observed features in the nebula, such as the present-day double-shell structure, and thermal instabilities (Rayleigh-Taylor and Kelvin-Helmholtz) along the dense shell. Nevertheless, the explosion scenario proposed by Smith et al.

**Table 1.** Models of  $\eta$  Car's Homunculi: Parameters of the colliding-outflows.

	Outflow Phase	$\lambda$	$v_1$ [km s <sup>-1</sup> ]	$v_2$ [km s <sup>-1</sup> ]	$\Delta t$ [yr]	$\dot{m}$ [M <sub>⊙</sub> yr <sup>-1</sup> ]
Run A	Standard wind	2.4	250	14	507	$1.0 \times 10^{-3}$
	Pre-outburst wind	1.9	500	14	20	0.7
	Explosion	1.9	1000	100	1	1.0
	Post-outburst wind	1.9	500	14	49	$1.0 \times 10^{-3}$
	Minor Eruption	1.9	200	10	10	$1.0 \times 10^{-2}$
	Post-outburst wind	1.9	500	300	120	$1.0 \times 10^{-3}$
Run B	Standard wind	2.4	250	14	507	$1.0 \times 10^{-3}$
	Pre-outburst wind	1.9	500	30	20	0.7
	Explosion	1.9	10000	100	1	0.1
	Post-outburst wind	1.9	500	14	49	$1.0 \times 10^{-3}$
	Minor Eruption	1.9	200	10	10	$1.0 \times 10^{-2}$
	Post-outburst wind	1.9	500	300	120	$1.0 \times 10^{-3}$

**Notes.** The 1890s minor eruption and post-eruptive wind conditions are taken from [González et al. \(2010\)](#).

(2003) could not account for the current physical size of the *large* Homunculus and, consequently, the estimated age of the nebula. It is noteworthy that these simulations do not include the high-velocity component of  $\sim 10000$  km s<sup>-1</sup> reported more recently by [Smith et al. \(2018a,b\)](#). In this work, we revisit 2D numerical simulations of the major eruption of  $\eta$  Car in the 1840s adopting the explosion scenario proposed by [Smith \(2013\)](#), including in our models this component of the outflowing gas.

The paper is organized as follows. In § 2, we describe the model. The numerical simulations and discussion of the results are presented in § 3. Finally, in § 4 we draw our conclusions.

## 2. The model

In this work, we assume the two-stage scenario for  $\eta$  Car's eruption proposed by [Smith et al. \(2018a\)](#): (1) a slow and massive wind phase expelled for a few decades before the 1840s, and (2) a lighter and faster explosive event. We have carried out two distinct models. In Run A, we have adopted an expansion speed of 1000 km s<sup>-1</sup> for Stage 2, while in Run B, an extremely high-velocity of 10000 km s<sup>-1</sup> is assumed for the explosion. According to [\(Smith et al. 2018a\)](#) from the circumstellar medium (CSM) interaction between the two stages, a dense and fast shell is produced that became the *large* Homunculus. Here, we explore such scenario and investigate whether it is able to explain not only the shape of the nebula, but also some of its observed physical properties, such as the latitude-dependent expansion speed and the estimated dynamical age. It is noteworthy that the formation of the internal nebula (commonly known as the *little* Homunculus) as well as the high-speed features in the equatorial skirt of  $\eta$  Car have been investigated in our previous works ([González et al. 2004a,b, 2010](#)).

For the different outflow phases, we have assumed the latitude-dependent ejection velocity and density proposed in [González et al. \(2010\)](#), that is,

$$v = v_1 F(\theta), \quad (1)$$

and,

$$n = n_0 \left(\frac{r_0}{r}\right)^2 \frac{1}{F(\theta)}, \quad (2)$$

respectively, where  $r_0$  is the injection radius, and  $F(\theta) = [(v_2/v_1) + e^{2z}]/[1 + e^{2z}]$  being  $z = \lambda \cos(2\theta)$  a function that controls the shape of the Homunculus. Equation (1) is a parametrization for the velocity of a latitude-dependent wind which that was first proposed by [Icke \(1988\)](#), and has been extensively used for modelling aspherical wind bubbles. The constant  $\lambda$  is related to the degree of asymmetry of the outflow, and  $\theta$  is the polar angle. The speed  $v_1$  is related to the expansion velocity  $v_p$  in the polar direction ( $\theta = 0^\circ$ ), while  $v_2$  to the corresponding value  $v_e$  at equator ( $\theta = 90^\circ$ ). From equations (1) and (2), it follows that a constant mass-loss rate per unit solid angle is assumed. It is worth mentioning that [González et al. \(2010\)](#) found the best fit to the observed expansion speed at different latitudes of  $\eta$  Car's Homunculus ([Smith 2006](#)) using  $\lambda = 1.9$ ,  $v_1 = 670$  km s<sup>-1</sup>,  $v_2 = 100$  km s<sup>-1</sup>. Using these parameters, the predicted expansion velocities are  $v_p = 657.5$  km s<sup>-1</sup> at the poles and  $v_e = 112.5$  km s<sup>-1</sup> in the equatorial direction (see Fig. 1 of [González et al. 2010](#)).

## 3. Numerical simulations

We performed new gas dynamic 2D numerical simulations of  $\eta$  Car's major eruption of the 1840s. The simulations were carried out with the adaptive grid Yguazú-A code developed by [Raga et al. \(2000\)](#). This code integrates the continuity, momentum and energy equations written in "conservation form". Also, the adaptive grid points are created using linear interpolations, which preserve the energy, mass and the momenta along the three coordinate axes. The problem that we are treating, though, is highly non-conservative due to the presence of a strong energy loss term. Different tests of the code have been reported by [Raga et al. \(2000, 2001\)](#); [Velázquez et al. \(2001\)](#).

The version of the code that has been used ([González 2018](#)) solves the gas dynamic equations explicitly accounting for the radiative cooling for the atomic/ionic species HI, HII, HeI, HeII, HeIII, CII, CIII, CIV, OI, OII, OIII, OIV. The cooling rates for the individual ions were calculated with the analytic approximations of [Raga et al. \(2002\)](#), which include the collisionally excited lines and collisional ionization (by free electrons), and a parametrized cooling rate for high temperatures. A set of rate equations is integrated together with the gas-dynamic equations to compute the non-equilibrium ionization state (with the ions listed above). The abundances (by number, relative to the total

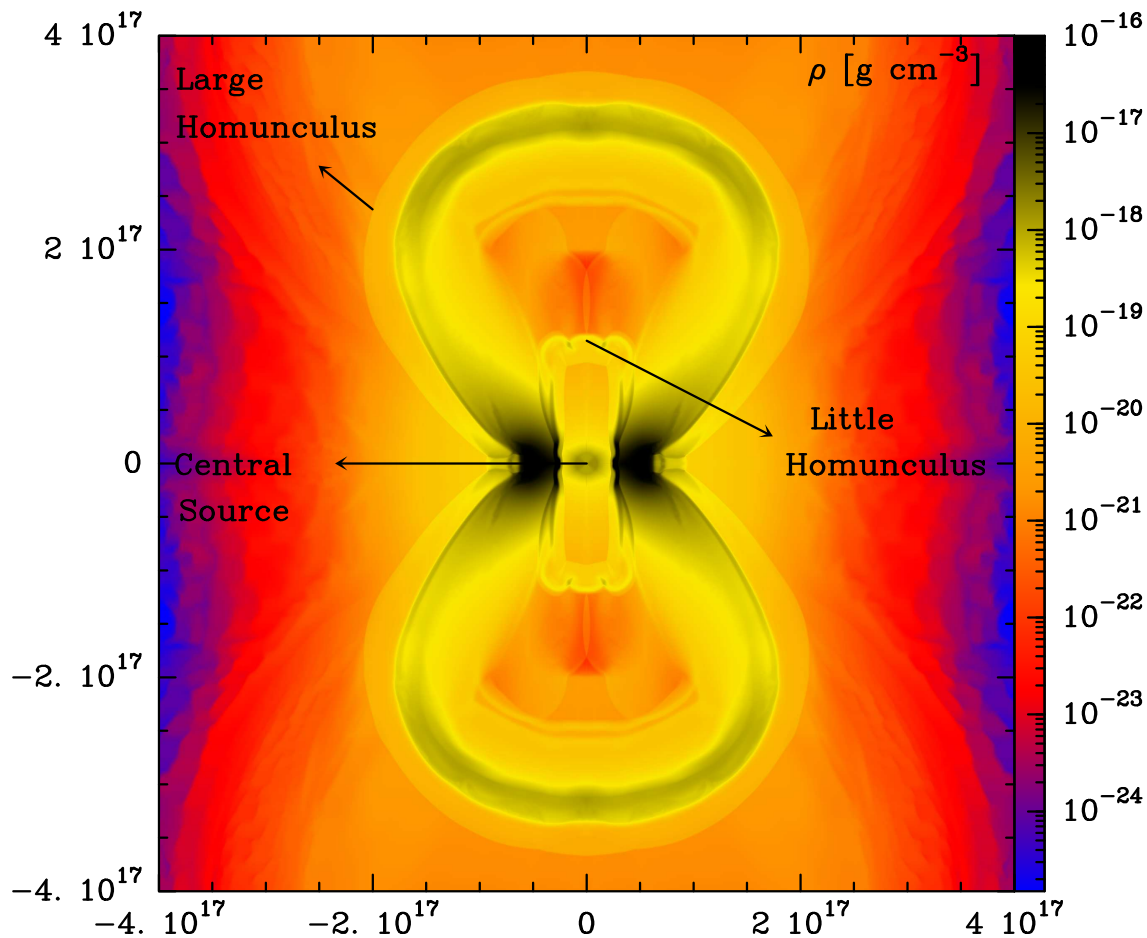


**Fig. 1.** Log-scale density stratification of  $\eta$  Car's nebulae. The numerical simulation (Run A) corresponds to an evolution time of  $t = 172$  yr since the great eruption in the 1840's. The bar at the right-side of the plot is in units of  $\text{g cm}^{-3}$ , and the computational domain axes are in units of cm. See the text for a physical description of the figure.

number of atoms) are of 0.9 (H), 0.1 (He),  $6.6 \times 10^{-4}$  (C) and  $3.3 \times 10^{-4}$  (O).

The calculations were axisymmetric and performed using the flux-vector splitting algorithm of van Leer (1982) on a five-level binary adaptive grid with a maximum resolution of  $3.9 \times 10^{14}$  cm along the two axes. The computational domain extends over  $(4 \times 10^{17}) \times (4 \times 10^{17})$ , which is initially filled by a homogeneous medium of density of  $10^{-3} \text{ cm}^{-3}$  and temperature of  $10^2$  K.

We should note that in our simulations we have assumed optically thin cooling, but the inner region of the Eta Carinae nebula are likely to be at least partially optically thick. We therefore overestimate the cooling rate (and therefore obtain lower temperatures) in the inner regions of the computed flow.

In Table 1, the models (Runs A-B) performed for  $\eta$  Car's major eruption are listed. In these models, the adopted parameters of the minor eruption and the winds expelled before and after this eruptive event are taken from González (2018). In addition, the physical conditions for the pre-eruptive wind and the explosion are consistent with the two-stage shock-powered event proposed by Smith et al. (2018a) for  $\eta$  Car's major eruption. In our numerical models, a standard wind with terminal velocity of  $v_0 = 250$

$\text{km s}^{-1}$  (in the polar direction) and mass-loss rate of  $\dot{M}_0 = 10^{-3} M_\odot \text{ yr}^{-1}$  is blown from a distance of  $r_0 = 10^{16}$  cm with a temperature  $T_0 = 10^5$  K into the unperturbed environment. Once the computational domain is filled by this wind, the double-stage of the major eruption occurs.

In Run A, the slow pre-outburst wind with an ejection velocity of  $500 \text{ km s}^{-1}$  (at the poles) and mass-loss rate of  $\dot{M} = 0.7 M_\odot \text{ yr}^{-1}$  is ejected during 20 yr, that results in a total mass of  $14 M_\odot$  expelled during this stage; and a brief explosion that lasts 1 yr, in which a mass of  $1 M_\odot$  is released with a speed of  $v = 1000 \text{ km s}^{-1}$  from the central source. Accordingly, the total kinetic energy released during the explosion is  $\sim 10^{49}$  erg, which is consistent with the estimated value of  $10^{49.7}$  by Smith (2013). Afterwards, a *post-outburst* wind with similar conditions of the current wind ( $v = 500 \text{ km s}^{-1}$  and  $\dot{M}_0 = 10^{-3} M_\odot \text{ yr}^{-1}$ ) is ejected until the minor eruption occurs, when the ejection velocity drops ( $200 \text{ km s}^{-1}$ ) and the mass-loss rate increases ( $\dot{M}_0 = 10^{-2} M_\odot \text{ yr}^{-1}$ ). Later, a post-eruption wind with  $v = 500 \text{ km s}^{-1}$  and  $\dot{M}_0 = 10^{-3}$  again resumes, and the *little* Homunculus is formed (Ishibashi et al. 2003). In our previous papers (González et al. 2004a, 2010) the formation and dynamical evolution of

the internal nebula has been investigated, and consequently, we focus here on the physical properties of the *large* Homunculus only.

Figure 1 depicts the predicted density distribution obtained from Run A of  $\eta$  Car's nebulae. The log-scale map at time  $t = 172$  yr after the major eruption is presented. It can be seen from the figure that the interaction of the different outflow phases produces internal and external nebulae which are consistent with the physical size and the shape of both Homunculi. For the large Homunculus we obtain a physical extension of the polar lobes of  $\pm 3.5 \times 10^{17}$  cm, expanding at a speed of  $\approx 600$  km s $^{-1}$ , which is close to the observed value of  $\approx 650$  km s $^{-1}$  of the Homunculus at high latitudes (Smith 2006). At the equator, the predicted physical size of the nebula across the star is  $\pm 9.1 \times 10^{16}$  cm expanding at  $\approx 140$  km s $^{-1}$ . In addition, as predicted in our previous work (González et al. 2010), the inner Homunculus shows the formation of instabilities (Rayleigh-Taylor and Kelvin-Helmholtz) along the polar caps due to the interaction of the lower density post-outburst wind that pushes and accelerates a higher density outflow (the 1890's minor eruption). After 172 yr of evolution, they expand at  $\approx 350$  km s $^{-1}$  extending from  $-1.1 \times 10^{17}$  cm to  $+1.1 \times 10^{17}$  cm along the major axis. It is worth mentioning that in González et al. (2004a, 2010), we showed that the interaction between both Homunculi in the equatorial zone results in the formation of tenuous, high-speed equatorial features ( $\sim 1000$  km s $^{-1}$ ) that seem to be related to the observed equatorial skirt of  $\eta$  Car nebulae. Notwithstanding, we note that these features are not produced in this numerical model, probably because the massive pre-outburst wind has a significant effect on such interaction. We have assumed in the simulation that  $14 M_{\odot}$ , of a total of  $15 M_{\odot}$  expelled during the two-stage scenario proposed by (Smith et al. 2018a) for  $\eta$  Car's eruption, are ejected during the pre-outburst wind. In contrast, the numerical models presented in González (2018) assumed  $10 M_{\odot}$  for each stage, which allows for the formation of the high-speed material at equator of  $\eta$  Car's lobes.

In Figure 2, we present the stratifications for Run A of the density of ionized hydrogen (top left), pressure (top right), temperature (bottom left) and velocity (bottom right) computed at an evolution time of  $t = 172$  yr after of the explosion phase. As we mentioned above, the simulation shows the formation of an external and internal nebulae which are in good agreement with the shape and kinematics of the large and the little Homunculi. The simulation shows a temperature of  $T \approx 10^4$  K behind the outer shock, while the mean temperature inside the shocked shell is  $T \approx 500$  K. In addition, it can be observed a low-density cavity between both Homunculi with temperature of  $T \approx 10$  K. On the other hand, no equatorial high-speed, low-density features that may be related to the observed equatorial skirt of  $\eta$  Car nebula are produced.

In Run B, we also assume a slow pre-outburst wind ejected for 20 yr with an ejection velocity of  $500$  km s $^{-1}$  (at the poles) and mass-loss rate of  $\dot{M} = 0.7 M_{\odot} \text{ yr}^{-1}$ . Afterwards, a brief explosion that lasts 1 yr occurs, during which a total mass of  $0.1 M_{\odot}$  is expelled from the central source with a speed of  $v = 10000$  km s $^{-1}$  (in the polar direction). It is worth mentioning that in this model we suppose for the explosive event a latitude-dependent mass-loss rate  $\dot{M} \propto F(\theta)$ , so the density  $n$  is not a function of  $\theta$  during this stage (see § 2). Adopting these parameters, the total kinetic energy released during the explosion is  $\sim 10^{50}$  erg, which is very close to the estimated value of  $10^{49.7}$  by Smith (2013) for the great eruption of  $\eta$  Car in the 1840s. The physical conditions for the subsequent outflow phases are the same as Run A. Accordingly, this numerical simulation includes the

high-speed component of  $10000$ - $20000$  km s $^{-1}$  for the explosion stage reported recently by Smith et al. (2018a,b). In addition, it is also remarkable that, as pointed out by these authors, most of the mass is ejected at slow speed in the pre-eruptive wind, while most of the kinetic energy is supplied by the fast material with much lower mass loss.

In Figure 3, we show the density map (in logarithmic scale) obtained from Run B at an evolution time  $t = 52$  yr since the explosive event. For this model, we have assumed for the great eruption a wide-angle explosive outflow with a speed  $v_1 = 10000$  km s $^{-1}$  and a speed  $v_2 = 100$  km s $^{-1}$  with most of the mass expelled toward the symmetry axis, such as it was proposed by Smith et al. (2018a). We note from the figure that this model has an important impact on the morphology and kinematics of  $\eta$  Car's nebulae. The assumed latitude-dependent flow parameters at injection are not able to account for the shape of the large Homunculus, that is, the outer expanding shell does not resemble its bipolar structure. Furthermore, the shocked layer expands too quickly, and therefore reaches the current physical size of  $\sim 3.5 \times 10^{17}$  cm (in the polar direction) at an evolution time  $t = 52$  yr since the explosion, long before the estimated kinematical age of  $\sim 175$  yr of the large Homunculus. On the other hand, the resulting expansion speed of  $\approx 1800$  km s $^{-1}$  at the poles is much greater than the observed value of  $\approx 650$  km s $^{-1}$  (Smith 2006). At the equator, the numerical simulation shows a physical size of the nebula of  $\pm 2.3 \times 10^{17}$  cm expanding at  $\approx 1200$  km s $^{-1}$ , which are not consistent with the corresponding observed values ( $\pm 3.1 \times 10^{16}$  cm and  $\approx 62$  km s $^{-1}$ ; Smith 2006). Besides, it is worth mentioning that important differences from our previous models (González et al. 2010; González 2018) are identified on the embedded structures. In particular, the simulation shows the formation of tenuous polar caps that may be related to the inner Homunculus, which results from the interaction of the minor eruption with its post-outburst wind. Nonetheless, these caps are located at a distance of  $\pm 2.7 \times 10^{16}$  cm from the central source, that does not correspond either to the current physical size of the *little* Homunculus of  $\pm 8 \times 10^{16}$  cm (Ishibashi et al. 2003; Smith 2006).

Figure 4 shows the density of ionized hydrogen (top left), pressure (top right), temperature (bottom left) and velocity (bottom right) maps computed for the interaction of the different outflows for Run B. The stratifications correspond to an evolution time of  $t = 52$  yr after of the explosion phase. As described above, the simulation shows that the outer shocked layer expands too fast reaching the observed physical size long before the estimated age of 175 yr of the large Homunculus. The simulation shows a temperature of  $T \approx 1.6 \times 10^4$  K behind the outer shock (in the polar direction), while the mean temperature inside the nebula is  $T \approx 200$  K. At the equator, outside the nebula, we see the presence of material with density of ionized hydrogen  $n_{HII} \approx 10^6$  cm $^{-3}$ , and temperature of  $T \approx 3 \times 10^3$  K, and at higher latitudes, the density decreases to  $n_{HII} \approx 1$  cm $^{-3}$  and the temperature increases to  $T \approx 2 \times 10^7$  K. In addition, the model predicts high speeds in the equatorial plane, with values increasing from  $v \approx 1000$  km s $^{-1}$  to  $v \approx 3000$  km s $^{-1}$ . At higher latitudes, the low-density material expands at a higher speed of  $v \approx 5000$  km s $^{-1}$ . Notwithstanding, no equatorial low-density features that may be related to the equatorial skirt of  $\eta$  Car nebula are observed.

## 4. Conclusions

In this article, new two-dimensional numerical models of the 1840s great eruption of  $\eta$  Car are presented. In contrast with our previous models which assume this eruption as a single explo-

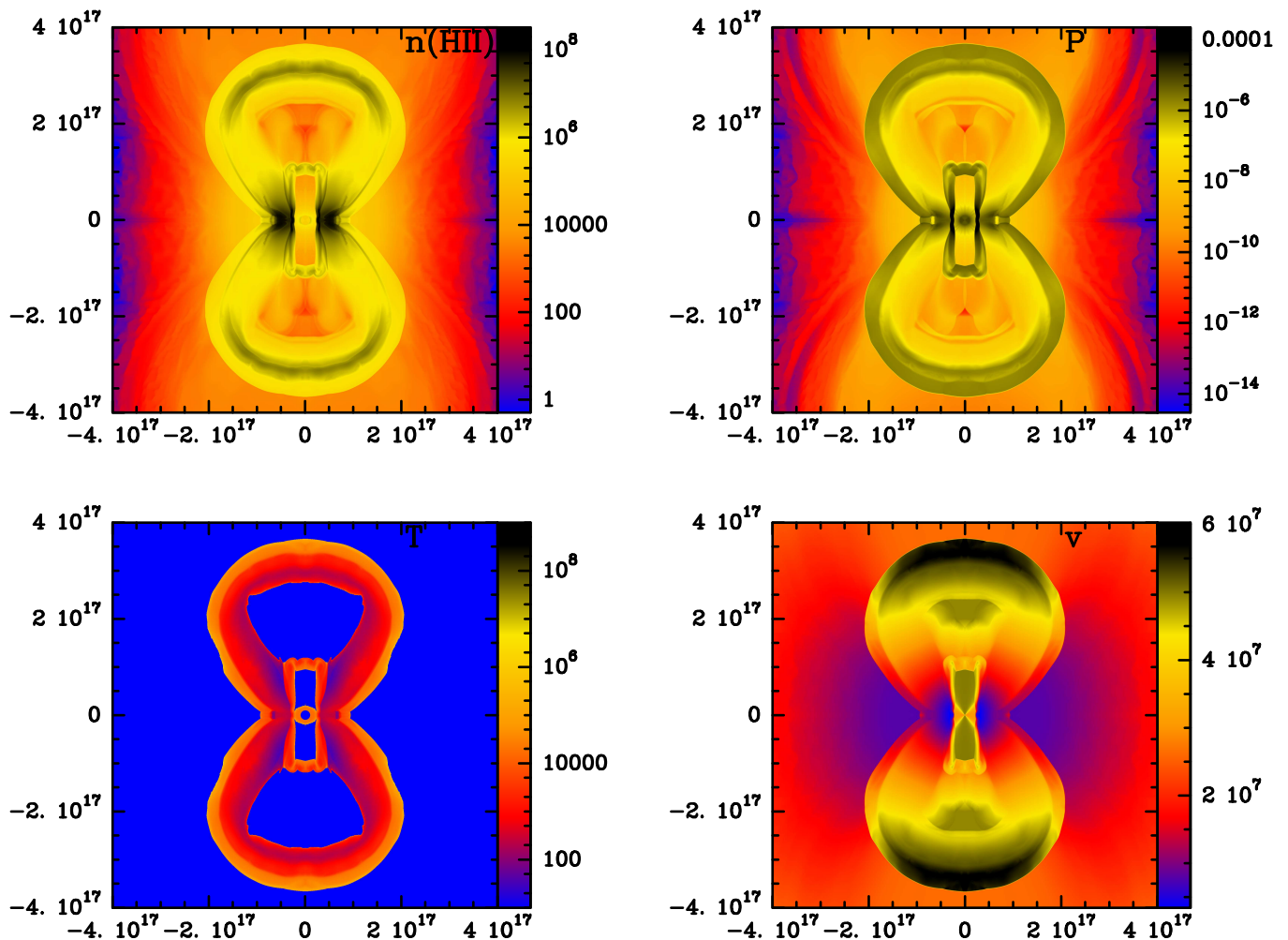


**Fig. 2.** Stratifications for Run A of density of ionized hydrogen (top left), pressure (top right), temperature (bottom left) and velocity (bottom right) computed 172 yr after the great eruption of  $\eta$  Car. The bars at the right-side of the panels are in units of  $\text{cm}^{-3}$ ,  $\text{dyn cm}^{-2}$ , K, and  $\text{cm s}^{-1}$ , respectively, and the computational domain axes are in units of cm. A further description of the figure is given in the text.

sion (González 2018), in the new high-resolution hydrodynamical simulations, we have incorporated the intermediate ( $500 \text{ km s}^{-1}$ ) and high-speed ( $10000 \text{ km s}^{-1}$ ) components proposed recently by Smith et al. (2018a,b). During this event, the energy injection was  $\sim 10^{49} - 10^{50}$  erg in which the parameters of  $\eta$  Car wind (ejection velocity and mass-loss rate) may have drastically changed in a very short period of time ( $\sim 1$  yr). Consequently, we have assumed here that the *large* Homunculus nebula may form from the interaction of this explosion with a previous stage wind of  $\eta$  Car (the CSM scenario proposed by Smith 2013). It is worth mentioning that we have not addressed the inner mechanism that triggered the explosive event. Potential processes are discussed in Smith et al. (2018a).

Adopting this scenario, our numerical simulation with an intermediate-speed explosion ( $1000 \text{ km s}^{-1}$ , Run A) was able

to explain both the shape and kinematics of the *large* Homunculus. In addition, the simulation predicts a kinematical age of the nebula of  $\sim 174$  yr that is consistent with the value estimated from observations ( $\sim 176$  yr). At this time of evolution, the predicted expansion velocity - along the symmetry axis - of the external shocked layer is of  $\approx 600 \text{ km s}^{-1}$ , which is very similar to the value of  $\approx 650 \text{ km s}^{-1}$  of the eta Car's Homunculus observed by Smith (2006). Furthermore, this model also shows the formation of the internal nebula (the *little* Homunculus) from the interaction of the minor eruption of the 1890s with the post-outburst wind, which, as in our previous models (González et al. 2004a, 2010) developed Rayleigh-Taylor instabilities that resemble the observed spatial structures in the polar caps (Smith 2005). Nonetheless, the high-speed equatorial features that may be related to the equatorial skirt of  $\eta$  Carinae are not produced.

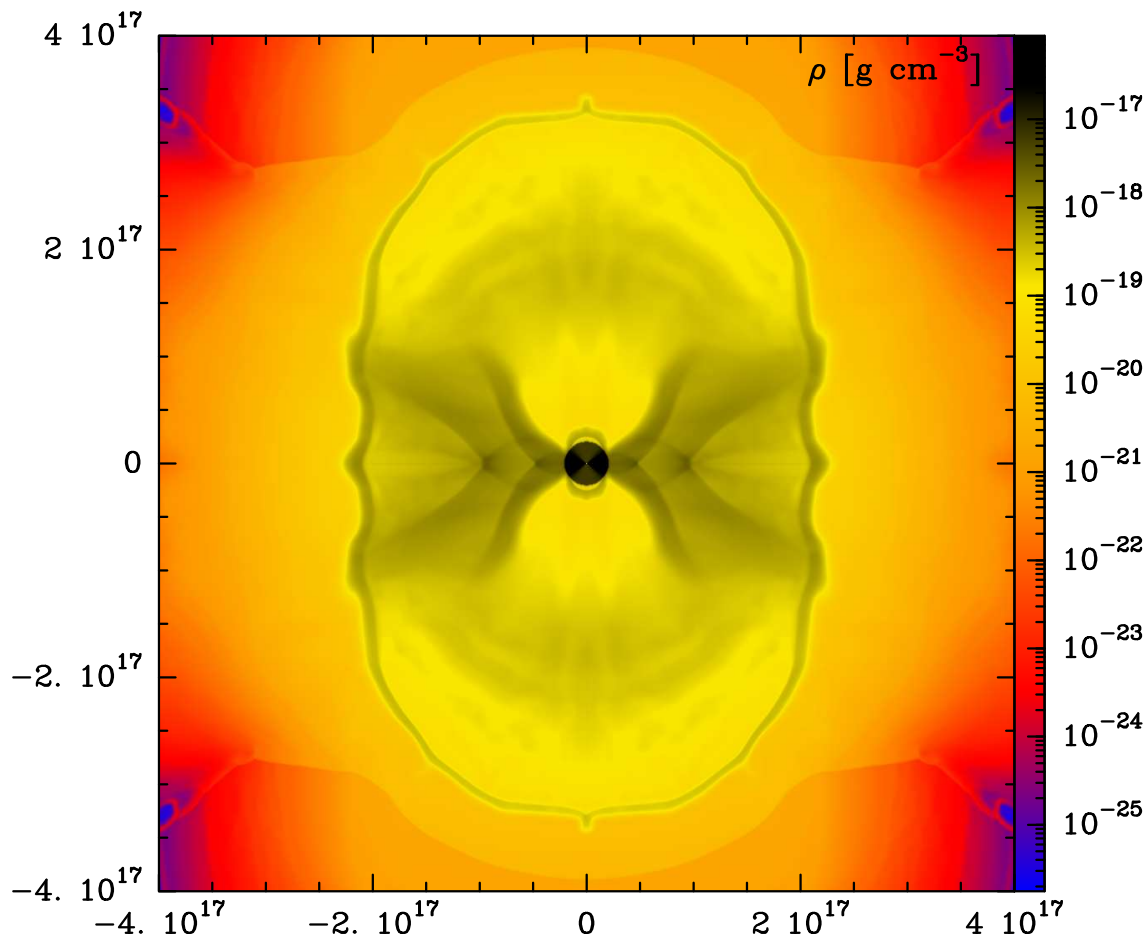


**Fig. 3.** Same as figure 1 of  $\eta$  Car’s nebulae for Run B after  $t = 52$  yr since the explosion. The bar at the right-side of the plot is in units of  $\text{g cm}^{-3}$ , and the computational domain axes are in units of cm. A physical description of the figure is given in the text.

On the other hand, the high-speed explosion numerical model ( $10000 \text{ km s}^{-1}$ , Run B) shows important differences both with regard to the morphology and dynamical evolution of the *large* Homunculus. First, the simulation predicts an outer shocked layer that does not resemble the bipolar structure of the nebula, and second, this layer expands too quickly (at a speed of  $\approx 1800 \text{ km s}^{-1}$ ) and, consequently, it reaches the observed physical size of the nebula ( $\sim 3.2 \times 10^{17} \text{ cm}$ ) -along the symmetry axis- at a time of 52 yr after the explosion, i.e. long before the estimated age of  $\sim 176$  yr of the *large* Homunculus. Besides, the numerical simulation shows important differences in the embedded structures. As expected, the model shows the formation of tenuous polar caps from the interaction of the minor eruptive event with the post-out burst wind, however, at this time of evolution, these structures are located at a distance of  $\pm 2.7 \times 10^{17} \text{ cm}$  from the source, and therefore do not reproduce the estimated extension of  $\pm 8 \times 10^{17} \text{ cm}$  of the polar caps of the *little* Homunculus. We should note that despite the differences in the parameters of Runs A and B, if we had employed the same values for the density profile, the general features obtained for the explosive model Run B would be essentially the same.

A final remark is that, in this work, we have focused in the shape and dynamical evolution of the *large* Homunculus assuming a high-speed,  $10000 \text{ km s}^{-1}$  explosion for the 1840s great eruption of  $\eta$  Car. One can ask whether an explosive event with speeds as high as  $10000 \text{ km s}^{-1}$  or larger is able to account for the observed physical properties of  $\eta$  Car’s nebula. We conclude from our numerical simulation that included this high-speed component (Run B) that this model can not reproduce the morphology or the age estimated from observations of the *large* Homunculus. On the other hand, a slower but also brief event with a velocity of  $1000 \text{ km s}^{-1}$  could nearly reproduce the observations.

*Acknowledgements.* RFG acknowledges financial support for UNAM-PAPIIT grant IN 107120. L.A.Z. acknowledges financial support from CONACyT-280775 and UNAM-PAPIIT IN110618 grants. ACR, JC, and PFV acknowledge the financial support for UNAM-PAPIIT grants IG 1000218 and IA10321. EMdGDP is grateful for the support from the Brazilian agencies FAPESP (grant 2013/10559-5) and CNPq (grant 308643/2017-8). The authors thank the anonymous referee for her/his useful comments and suggestions that improved the content of this work.

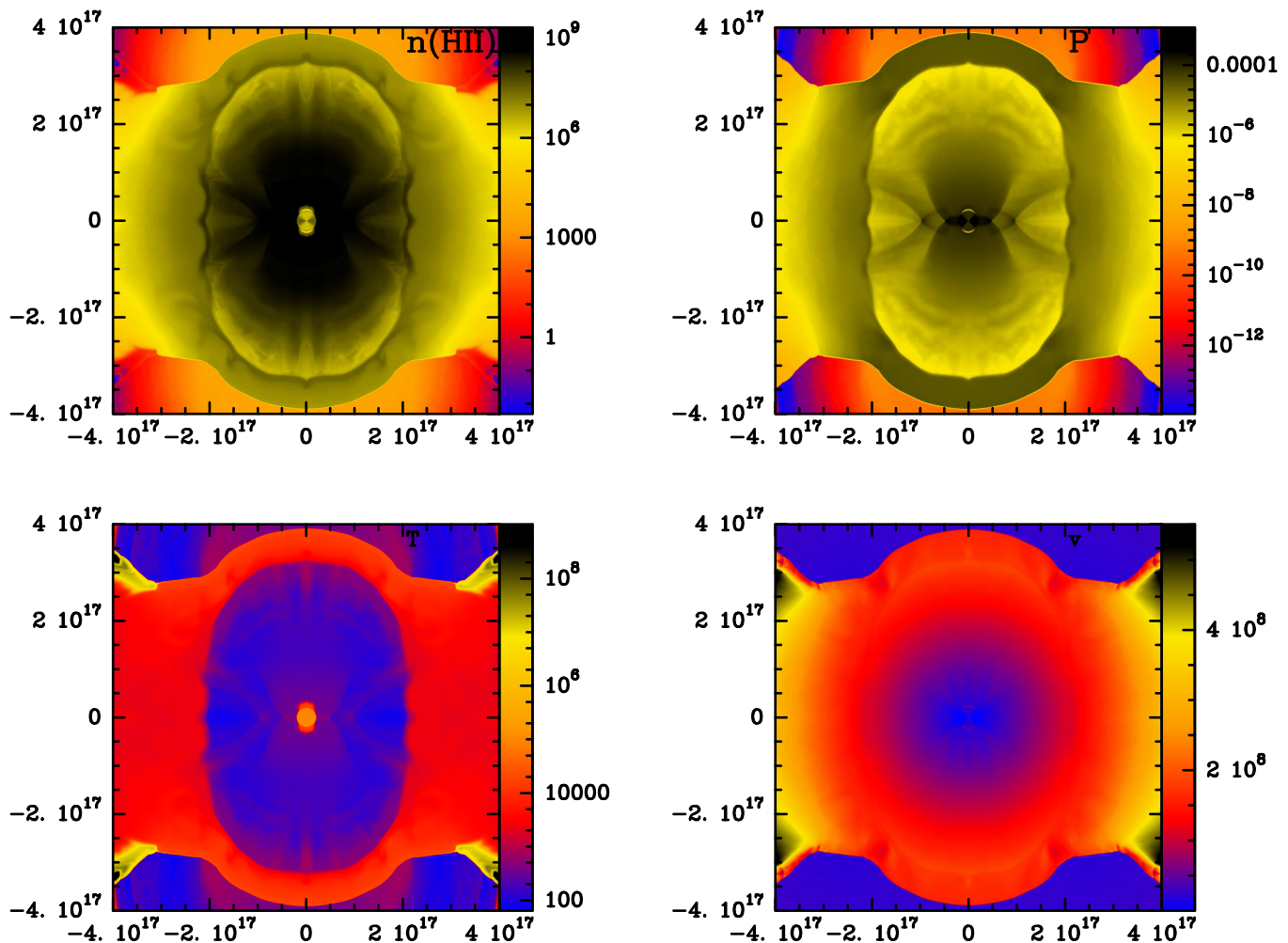


**Fig. 4.** Stratifications for Run B of density of ionized hydrogen (top left), pressure (top right), temperature (bottom left) and velocity (bottom right) computed 52 yr after the great eruption of  $\eta$  Car. The bars at the right-side of the panels are in units of  $\text{cm}^{-3}$ ,  $\text{dyn cm}^{-2}$ , K, and  $\text{cm s}^{-1}$ , respectively, and the computational domain axes are in units of cm. A further description of the figure is given in the text.

## References

- Abraham, Z., Falceta-Gonçalves, D., & Beaklini, P. P. B. 2014, *ApJ*, 791, 95. doi:10.1088/0004-637X/791/2/95
- Davidson, K., & Humphreys, R. M. 1997, *ARA&A*, 35, 1
- Davidson, K., Smith, N., Gull, T. R., et al. 2001, *AJ*, 121, 1569. doi:10.1086/319419
- Humphreys, R. M., Davidson, K., & Smith, N. 1999, *PASP*, 111, 1124. doi:10.1086/316420
- Icke, V. 1988, *A&A*, 202, 177
- Ishibashi, K., Gull, T. R., Davidson, K., et al. 2003, *AJ*, 125, 3222. doi:10.1086/375306
- González, R. F. 2018, *A&A*, 609, A69
- González, R. F., Villa, A. M., Gómez, G. C., et al. 2010, *MNRAS*, 402, 1141. doi:10.1111/j.1365-2966.2009.15950.x
- González, R. F., de Gouveia Dal Pino, E. M., Raga, A. C., et al. 2004, *ApJ*, 616, 976. doi:10.1086/425112
- González, R. F., de Gouveia Dal Pino, E. M., Raga, A. C., et al. 2004, *ApJ*, 600, L59. doi:10.1086/381390
- Kashi, A., & Soker, N. 2009, *New A*, 14, 11
- Morris, P. W., Waters, L. B. F. M., Barlow, M. J., et al. 1999, *Nature*, 402, 502.
- Smith, N., Andrews, J. E., Rest, A., et al. 2018, *MNRAS*, 480, 1466.
- Smith, N., Rest, A., Andrews, J. E., et al. 2018, *MNRAS*, 480, 1457.
- Smith, N. 2013, *MNRAS*, 429, 2366. doi:10.1093/mnras/sts508
- Smith, N. 2006, *ApJ*, 644, 1151
- Smith, N. 2005, *The Fate of the Most Massive Stars*, 332, 307
- Smith, N., Gehrz R. D., Hinz P. M., Hoffmann W. F., Hora J. L., Mamajek E. E., Meyer M. R., 2003, *AJ*, 125, 1458
- Owocki, S. P., & Shaviv, N. J. 2016, *MNRAS*, 462, 345
- Portegies Zwart, S. F., & van den Heuvel, E. P. J. 2016, *MNRAS*, 456, 3401.
- Raga, A. C., Navarro-González, R., & Villagrán-Muniz, M. 2000, *Rev. Mexicana Astron. Astrofis.*, 36, 67
- Raga, A. C., Villagrán-Muniz, M., Navarro-González, R., Masciadri, E. 2001, *RMxAA*, 37, 87
- Raga, A. C., de Gouveia Dal Pino, E. M., Noriega-Crespo, A., Mininni, P. D., Velázquez, P. F. 2002, *A&A*, 392, 267
- van Leer, B. 1982, *Numerical Methods in Fluid Dynamics*, 507. doi:10.1007/3-540-11948-5\_66

Velázquez, P. F., Sobral, H., Raga, A. C., Villagrán-Muniz, M., Navarro-González, R. 2001, *RMxAA*, 37, 87  
Woosley, S. E. 2017, *ApJ*, 836, 244